Astron. Astrophys. 348, 189–197 (1999)

ASTRONOMY AND ASTROPHYSICS

Analysis of ultraviolet and extreme-ultraviolet spectra of the DA white dwarf G 191-B2B using self-consistent diffusion models⋆

S. Dreizler[1] **and B. Wolff**[2]

[1] Institut für Astronomie und Astrophysik, Universität Tübingen, D-72076 Tübingen, Germany (dreizler@astro.uni-tuebingen.de)
[2] Institut für Theoretische Physik und Astrophysik, Universität Kiel, D-24098 Kiel, Germany (wolff@astrophysik.uni-kiel.de)

Received 2 February 1999 / Accepted 21 May 1999

Abstract. We present a multi–wavelength spectral analysis of the DA white dwarf G 191-B2B. The employed atmospheric models account for gravitational settling and radiative levitation, which are, for the first time, calculated self-consistently with the atmospheric structure. The resulting spectra can reproduce the complete EUVE spectrum and the ultraviolet lines of iron. Some restrictions regarding the UV lines of other elements (C, N, O, Ni), however, still remain. In contrast to homogeneous models, it is not necessary to introduce additional photospheric or interstellar absorbers to account for the high opacity at $\lambda \lesssim 230$ Å. Abundance profile changing mechanisms, like mass-loss or accretion, are also not needed.

Key words: stars: abundances – stars: atmospheres – stars: evolution – stars: individual: G 191-B2B – stars: white dwarfs – ultraviolet: stars

1. Introduction

The chemical composition of white dwarf atmospheres is determined mainly by the high surface gravity ($\log g \approx 8$) of these stars: Chemical elements are sorted according to their weight. The lightest element, either hydrogen or helium, diffuses on top of the atmosphere and dominates the optical spectrum. However, this simple picture is altered if competing mechanisms are present. In the case of white dwarfs hotter than 20 000 K the most important process is selective radiative pressure (radiative levitation). Theoretical calculations by Vauclair et al. (1979) and later by Morvan et al. (1986), Vauclair (1987, 1989), and Chayer et al. (1989, 1991, 1994, 1995a, 1995b) have shown that radiative acceleration can be strong enough at some effective temperatures and gravities to provide traces of photospheric elements such as carbon, nitrogen, oxygen, silicon, iron, and nickel. Recently, Unglaub & Bues (1998) investigated the influence of a weak stellar wind on the element stratification of hot white dwarfs ($T_{\rm eff} \gtrsim 65\,000$ K).

Theoretical predictions of abundances for trace elements have been tested by numerous observations in the ultraviolet, extreme-ultraviolet, and X-ray regions of the electromagnetic spectrum. The basic results for hydrogen rich white dwarfs (spectral type DA) are ambiguous: On the one hand, the general increase in EUV opacity at $T_{\rm eff} \gtrsim 50\,000$ K, as observed by ROSAT and EUVE, is consistent with an increase of predicted iron and nickel abundances (e.g. Barstow et al. 1993, Jordan et al. 1994, Wolff et al. 1996, Barstow et al. 1997, Marsh et al. 1997, Wolff et al. 1998). On the other hand, individual abundances for several elements cannot be reproduced (e.g. Chayer et al. 1995a). Moreover, radiative levitation seems to be only of minor importance at $T_{\rm eff} \lesssim 50\,000$ K (e.g. Barstow et al. 1996b, Holberg et al. 1997, Wolff et al. 1998, 1999a).

The major drawbacks of all the previous work are the assumption of a fixed flux distribution for the calculation of the radiative forces and the calculation of the theoretical spectra with a homogeneous distribution of trace elements. These shortcomings can now be relaxed by calculating the atmospheric structure, the radiation field, and the element distribution self-consistently (Dreizler 1999).

An important role for the understanding of diffusion and radiative levitation plays the DA white dwarf G 191-B2B ($T_{\rm eff} \approx 56\,000$ K). It is relatively bright and has been frequently used as calibration standard for UV/EUV satellites with numerous observations in these wavelength ranges. Photospheric lines from C, N, O, Si, P, S, Fe, and Ni could be identified in observations with the IUE (Bruhweiler & Kondo 1981, Vennes et al. 1992, Holberg et al. 1994, Werner & Dreizler 1994), HST (Sion et al. 1992, Vidal-Madjar et al. 1994, Wolff et al. 1998), and ORFEUS (Vennes et al. 1996) satellites. These detections could be used to reproduce the general shape of the EUVE spectrum (Koester 1996, Barstow et al. 1996a, Lanz et al. 1996, Wolff et al. 1997, 1998) demonstrating that the absorption features in the UV and EUV regions are largely caused by the same elements. In detail, the most important elements for the EUV opacity turned out to be iron and nickel (Lanz et al. 1996, Wolff et al. 1998).

Although the general shape of the EUVE spectrum could be reproduced using homogeneous abundances from UV observations, Lanz et al. (1996) and Wolff et al. (1998) had to include

Send offprint requests to: S. Dreizler

⋆ Based on observations made with the EUVE Sattelite and with the NASA/ESA Hubble Space Telescope, obtained from the data archive at the Space Telescope Science Institute. STScI is operated by the Association of Universities for Research in Astronomy, Inc. under NASA contract NAS 5-26555.

small amounts of additional helium, either photospheric or interstellar, to improve the fit at $\lambda < 230$ Å. In order to remove this problem, Barstow & Hubeny (1998) suggested a stratified H+He envelope whereas Barstow et al. (1999) used an ad hoc stratification of iron. Barstow et al. also proposed weak mass-loss to account for the lower iron abundance in the outer layers.

In this paper we demonstrate that our new self-consistent diffusion models are able to reproduce UV and EUV spectra of G 191-B2B with only $T_{\rm eff}$ and $\log g$ as free parameters. In Sect. 2 we present a short description of these models. The analysis of the observations is presented in Sect. 3 and discussed in Sect. 4.

2. Self-consistent diffusion models

2.1. General remarks

As discussed in the introduction, the strong gravitational field together with very low mass loss rates and the absence of convective turbulence efficiently drives a gravitational sedimentation process in white dwarfs. These diffusion processes determine the spectral appearance of white dwarfs and are therefore important for our understanding of the evolution of white dwarfs.

Diffusion time scales within the atmospheres of hot white dwarfs are extremely small compared to the evolutionary time scale (e.g. Koester 1989). The downward force is counteracted by radiative acceleration provided by the outward directed radiation flux transferring momentum to the plasma by absorption processes. Changing physical parameters within the atmosphere (degree of ionization, intensity of the radiation field) makes the radiative cross sections of each element depth dependent and therefore the interaction between gravitational settling and radiative acceleration leads to an abundance stratification within the envelope. The distribution within the atmosphere of all elements show pronounced stratifications (Figs. 1, 2), for example, enough momentum from the radiation field can be transfered to iron via the millions of spectral lines over two decades in $\tau_{\rm ross}$ within the line forming region. The resulting equilibrium abundance is nearly homogeneous and very close to the one determined from homogeneous models (Lanz et al. 1996, Wolff et al. 1998). This is the reason why the fit with homogeneous models is quite successful, however, not perfect. In the outer regions the abundance drops sharply since no force can balance gravitational settling. Interestingly, this is qualitatively similar to the ad hoc Fe stratification used by Barstow et al. (1999). However, our model requires no free parameter and no mass loss (see also Sect. 4). For comparison, we derived the abundance at $\tau_{\rm ross} = 2/3$ and list it together with the corresponding values of Chayer et al. (1995b) in Table 1.

Assuming the absence of concurring processes like convection and mass loss the short diffusion time scale justifies to determine the equilibrium abundances of the trace elements[1] at each depth point from the balance of gravitational, radiative and electrical forces. Our approach (see next subsection) is therefore very similar to that of Chayer et al. (1995a) and earlier work of this group, however, we perform for the first time self-consistent diffusion calculations under NLTE-conditions, i.e., considering the back-reaction of the element stratification on the atmospheric structure. In this approach, the only free parameters are the effective temperature and the surface gravity. Wolff et al. (1998) have determined $T_{\rm eff} = 56\,000$ K and $\log g = 7.6$ from an analysis of optical and EUVE spectra of G 191-B2B. These determinations are mainly based on the fit of the optical hydrogen lines, which are not affected by the chemical stratification, but include the blanketing effect from the numerous EUV lines. In order to investigate the influence of these two input parameters we also varied $T_{\rm eff}$ and $\log g$ within reasonable error limits (± 3000 K, ± 0.2 dex). Within these limits, an increase/decrease of $T_{\rm eff}$ has the same effect as a decrease/increase of $\log g$, namly an increase/decrease of the abundance of 0.2 dex (Figs. 2, 3, 4).

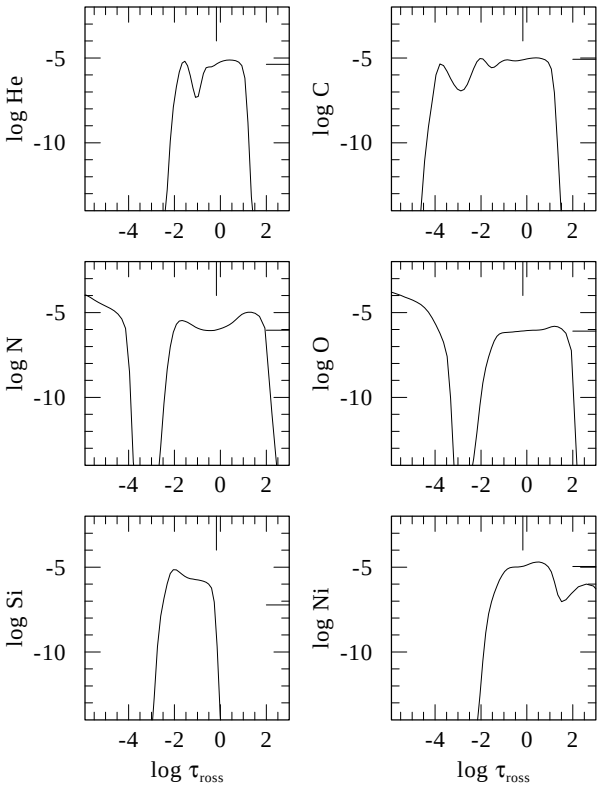

Fig. 1. Distribution of elements (number fraction) over the Rosseland optical depth in the atmosphere ($T_{\rm eff}$=56 000 K, $\log g = 7.6$). The abundance at $\tau_{\rm ross} = 2/3$ is indicated at the right (see also Table 1)

Table 1. Logarithmic abundances at $\tau_{\rm ross} = 2/3$

Element	this work	Chayer et al. (1995b)
He	-5.4	
C	-5.1	-5.0
N	-6.0	-5.3
O	-6.1	-5.3
Si	-7.2	-7.6
Fe	-4.9	-5.3
Ni	-5.0	

[1] The main constituent, in this case hydrogen, is assumed to be distributed homogeneously.

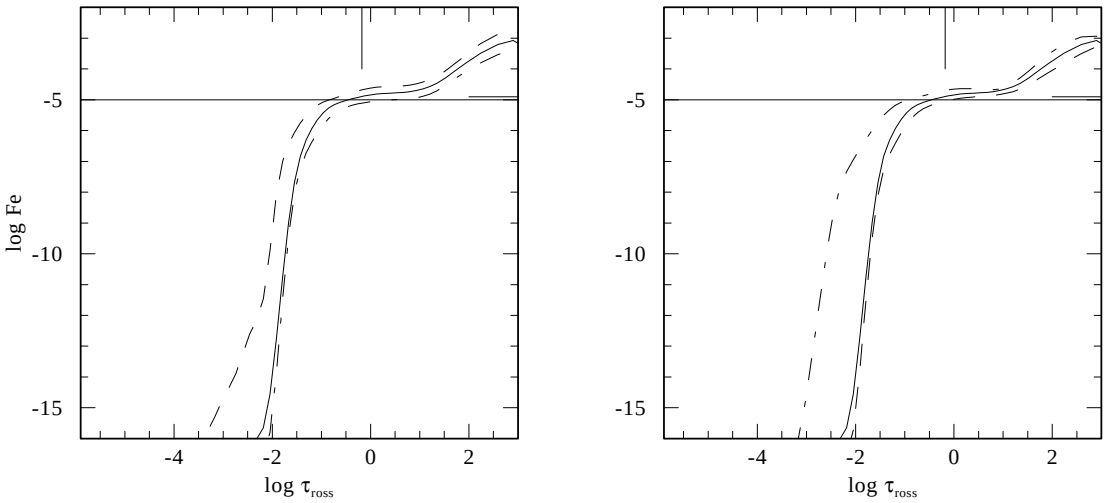

Fig. 2. Dependence of the Fe distribution (number ratio) over the Rosseland optical depth of $\log g$ (*left*) and $T_{\rm eff}$ (*right*). Left $T_{\rm eff}$=56 000 K: $\log g = 7.4$ (dashed), $\log g = 7.6$ (full), and $\log g = 7.8$ (dash-dotted). Right $\log g$=7.6: $T_{\rm eff}$=53 000 K (dash-dotted), $T_{\rm eff}$=56 000 K (full), and $T_{\rm eff}$=56 000 K (dashed). The homogeneous Fe abundance of the best fitting homogeneous model of Wolff et al. (1998) is indicated as a straight line. The abundance at $\tau_{\rm ross} = 2/3$ is indicated at the right (see also Table 1)

2.2. Outline of the model calculations

The short diffusion time scale in combination with the absence of convection and mass loss allows the determination of abundances at each depth point from the balance of gravitational, radiative and electrical forces. For a trace element (i) in a plasma mainly composed of element (1) this can be written as:

$$\begin{aligned} m_1F_1 - m_iF_i &= (A_i - A_1)m_{\rm p}g - (Z_i - Z_1)eE \\ &\quad -A_i m_{\rm p} g_{{\rm rad},i} \\ &= 0. \end{aligned} \tag{1}$$

A_i are the atomic weights, Z_i the mean electrical charges, m_p is the proton mass, and $g_{{\rm rad},i}$ is the radiative acceleration acting on element (i). Neglecting the radiative forces on element (1) assumes that the main constituent of the plasma is homogeneously distributed over the atmosphere (however, still hydrostatically stratified). The radiative acceleration is given by

$$g_{{\rm rad},i} = \frac{1}{\rho_i}\frac{4\pi}{c}\int_0^\infty \kappa_{\nu,i} H_\nu {\rm d}\nu \tag{2}$$

where ρ_i is the mass fraction of the element (i), $\kappa_{\nu,i}$ is the frequency dependent mass absorption coefficient which includes all contributions of this element at the frequency ν, and H_ν is the Eddington flux. The electric field E can be obtained from charge conservation:

$$\sum P_j Z_j = P_{\rm e} \tag{3}$$

where P_j and $P_{\rm e}$ denote the partial pressure of the elements (j) and of the electrons, respectively. Differentiating Eq. (3) with respect to r and inserting the partial pressures P_i as given by

$$\frac{1}{P_i}\frac{{\rm d}P_i}{{\rm d}r} = \frac{A_i m_{\rm p} g}{kT} + \frac{Z_i eE}{kT}$$

results after some simplifications in

$$eE = \frac{A_1 m_{\rm p} g}{Z_1 + 1}.$$

With this expression Eq. (1) reads

$$\begin{aligned} m_1F_1 - m_iF_i &= m_{\rm p}g\left(A_i - A_1 - \tfrac{Z_iA_1}{Z_1+1} + \tfrac{Z_1A_1}{Z_1+1}\right) \\ &\quad -A_i m_p g_{\rm rad} \\ &= A_i m_{\rm p}\left(\left(1 - \tfrac{A_1(Z_i+1)}{A_i(Z_1+1)}\right)g - g_{{\rm rad},i}\right) \\ &= 0. \end{aligned} \tag{4}$$

With

$$g_{{\rm eff},i} := \left(1 - \frac{A_1(Z_i+1)}{A_i(Z_1+1)}\right) g$$

Eq. (4) yields:

$$g_{{\rm rad},i} = g_{{\rm eff},i} \tag{5}$$

which is exactly what Chayer et al. (1995a) derived. Eq. (5) defines the mass fraction of element (i) at each depth point through the dependence of the radiative acceleration on ρ_i (Eq. 2).

In contrast to the necessity in homogeneous model atmospheres, the opacity has to be determined accounting for Stark broadening of every line. Additionally, the model atoms have to be very detailed in order to provide a realistic amount of radiative acceleration. In the current stage, we ignore possible effects from redistribution of the transfered momentum over the ionization stages. We also assume that a bound-free transition transfers the momentum completely to the ion ignoring a momentum transfer to the electron.

Since the equilibrium condition (5) is coupled via the opacity and the Eddington flux to the structure of the model atmosphere, it must be solved self-consistently with our usual set of equations necessary for the construction of non–LTE model atmospheres. We perform this in the most simple way by an iterative scheme. Starting with a homogeneous atmosphere we take its radiation field, density and temperature stratification as well as the occupation numbers of all atomic energy levels and calculate the

Table 2. Summary of observations

Instrument	Data set	Exp. time [sec]
STIS/HST	O4PG02QCQ	2160
	O4PG02QKQ	3091
	O4VT02NJQ	2160
	O4VT02NYQ	3096
	O57U01020	2040
Instrument	Observation dates	Exp. times [ksec] (SW, MW, LW)
EUVE	1993/10/28–10/30	53.2, 47.8, 50.4
	1993/12/07–12/08	26.1, 20.1, 24.2
	1994/03/05–03/08	45.8, 43.7, 44.1

radiative acceleration of all elements at all depth points. We then solve Eq. (5) obtaining a chemical stratification for all trace elements. Keeping this fixed, we re-determine the structure and the radiation field for the next iteration step. Alternatively the equilibrium condition could be included as an additional constraint equation in the construction of the model atmosphere which in principle would result in a faster convergence. However, starting from the chemically homogeneous models would then be nearly impossible, due to large initial changes in the abundances and therefore in the atmospheric structure.

3. Analysis of observed spectra

3.1. HST spectra

While the EUVE spectra of hot white dwarfs are sensitive to the overall flux distribution the spectral resolution is too low to identify individual metal lines. This requires UV spectroscopy allowing to determine the abundances of heavier elements. The STIS spectrograph on-board the Hubble Space Telescope is the best suited instrument. It covers a wide spectral range at high resolution. We therefore have retrieved all available STIS spectra of G 191-B2B covering the wavelength range between 1200 and 1450 Å (see Table 2). In order to produce a merged spectrum the individual orders were normalized and then co-added. For this purpose we degraded the higher resolution of the O57U01020 data set ($\lambda/\delta\lambda = 114\,000$) down to the resolution of the others ($\lambda/\delta\lambda = 45\,800$). The result is an excellent UV spectrum of G 191-B2B providing a very strong constraint for our new model atmospheres. For comparison, we also retrieved all available IUE spectra from the final archive and produced a combined spectrum. However, the quality is much poorer compared to the combined STIS spectrum so that we did not take these data into account.

The UV lines calculated from the diffusion model are compared with the observations in Fig. 3. Good agreement is achieved for the Fe V lines whereas Ni V is somewhat too strong. As demonstrated in Figs. 3 and 4 the line strength of Ni V can be reduced with a slight increase in $\log g$ or a slight decrease in $T_{\rm eff}$. It should also be noted that this deviation is only visible in the excellent STIS spectrum and that the atomic data, mainly the bound-free radiative cross sections, which contribute to the radiation force, are poorly known. The Ni abundance is therefore correctly reproduced within the uncertainty limit of our models. We also observe discrepancies for C, N, O, and Si, which can be partly compensated be moderate changes in $T_{\rm eff}$ and $\log g$, too. In order to estimate the significance of these deviations we have also calculated models with artificially changed total abundances. The abundance distribution of each element is held fixed but the overall abundance is multiplied by factors 0.02 for carbon, 0.1 for nitrogen, 0.5 for oxygen, 5 for silicon and 0.2 for nickel. Now, the lines of all element agree well (Fig. 5). For all elements except carbon these corrections are within a factor of ten and can also be attributed to uncertainties of our models. Main uncertainty is the treatment of the re-distribution of the momentum of individual ions onto the surrounding plasma (see also the discussion of Dreizler 1999). The reason for the larger deviation of carbon remains to be investigated.

In agreement with the previous analysis of Werner & Dreizler (1994), the Ni/Fe abundance ratio in our diffusion model is of the order of one over the whole atmosphere. Werner & Dreizler interpreted this large deviation from the solar ratio as clear indication for diffusion processes, which can now be modeled reliably.

3.2. EUVE spectra

The EUVE spectra of G 191-B2B were obtained from the public archive. Table 2 summarizes the observations. The spectra were reduced, flux calibrated and subtracted from contributions of higher orders with the standard procedures of the IRAF/EUV package. For the LW spectrometer we applied the correction factors of Dupuis et al. (1995) for the second, third, and fourth orders. Finally, the individual spectra were co-added according to the exposure times.

For a comparison with the observations, the synthetic spectrum is normalized to the visual magnitude of $V = 11.79$. Interstellar absorption is calculated according to the model of Rumph et al. (1994). From the region around the He I edge at 504 Å we determine $N(\mathrm{HI}) = 2.11 \cdot 10^{18}\,\mathrm{cm}^{-2}$ and $\mathrm{He\,I/H\,I} = 0.067$, similar to previous analyses (e.g. Dupuis et al. 1995). For He II we assume the mean value of $\mathrm{He\,II/H\,I} = 0.052$ from the interstellar analysis of EUVE spectra by Wolff et al. (1999b).

In Fig. 6 we compare the synthetic spectrum from the diffusion model with the EUVE observation. The flux distribution is well reproduced over the whole spectral range. The main deviations appear at the long wavelengths tail where the subtraction of higher order contributions is uncertain. At shorter wavelengths, there are several strong absorption features in the model spectrum which are not in that strengths visible in the observation.

The improvement compared to models with homogeneous element distributions can be seen from Fig. 7. In this figure, we plot the best fitting NLTE spectrum from Wolff et al. (1998) together with the EUVE observation. Effective temperature and gravity are identical with the diffusion model. In order to facilitate the comparison, we have also used the same interstellar parameters as for Fig. 6.

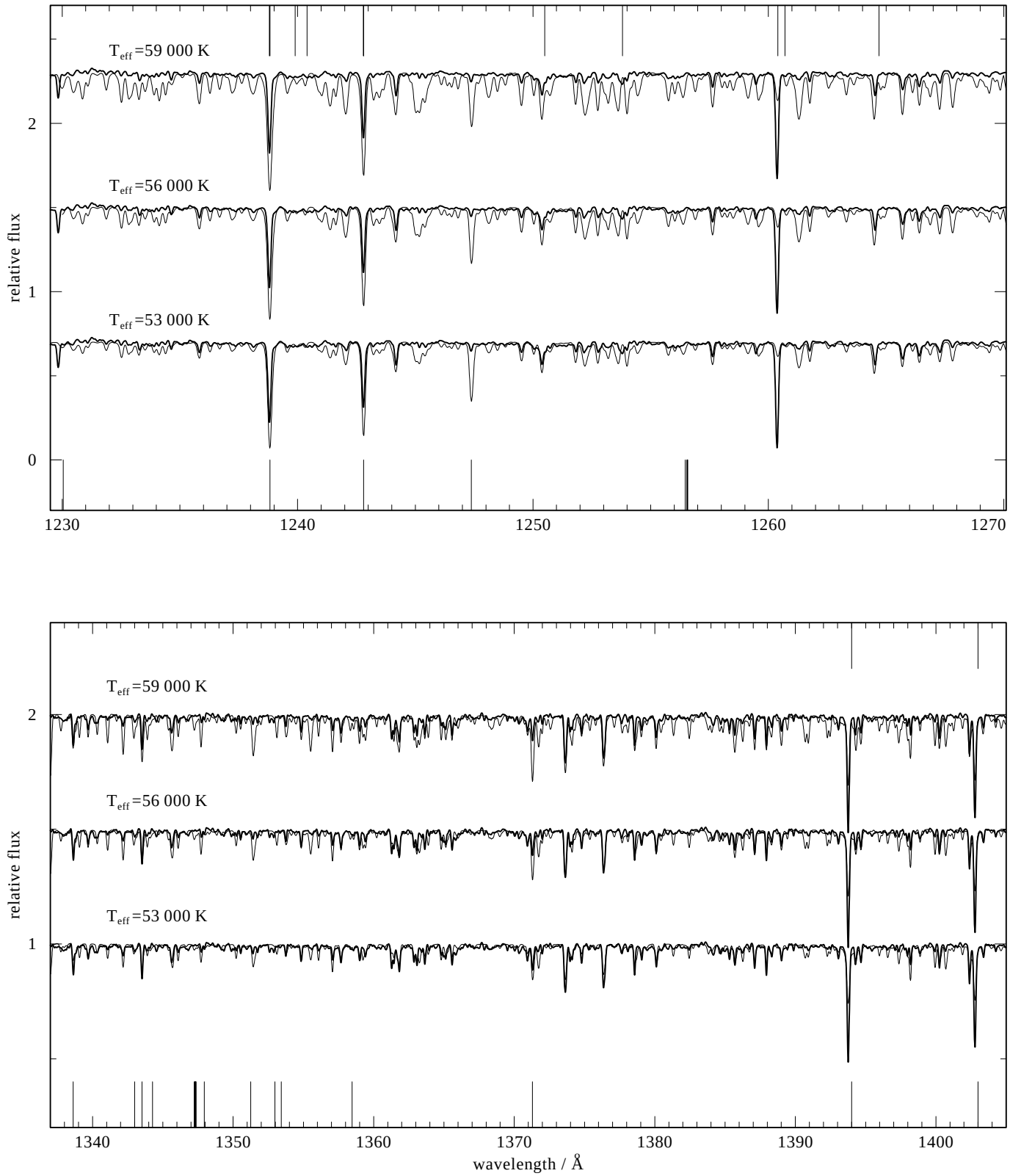

Fig. 3. Combined STIS spectrum of G 191-B2B (thick line) compared to our self-consistent NLTE model atmospheres ($T_{\rm eff}$=56 000 K) with three surface gravities (from *top* to *bottom* in each plot $\log g = 7.4, 7.6, 7.8$): *Upper plot:* region dominated by Ni V lines; lower plot: region dominated by Fe V lines. Interstellar lines are indicated at the *top*, stellar C, N, O, and Si lines are indicated at the *bottom*

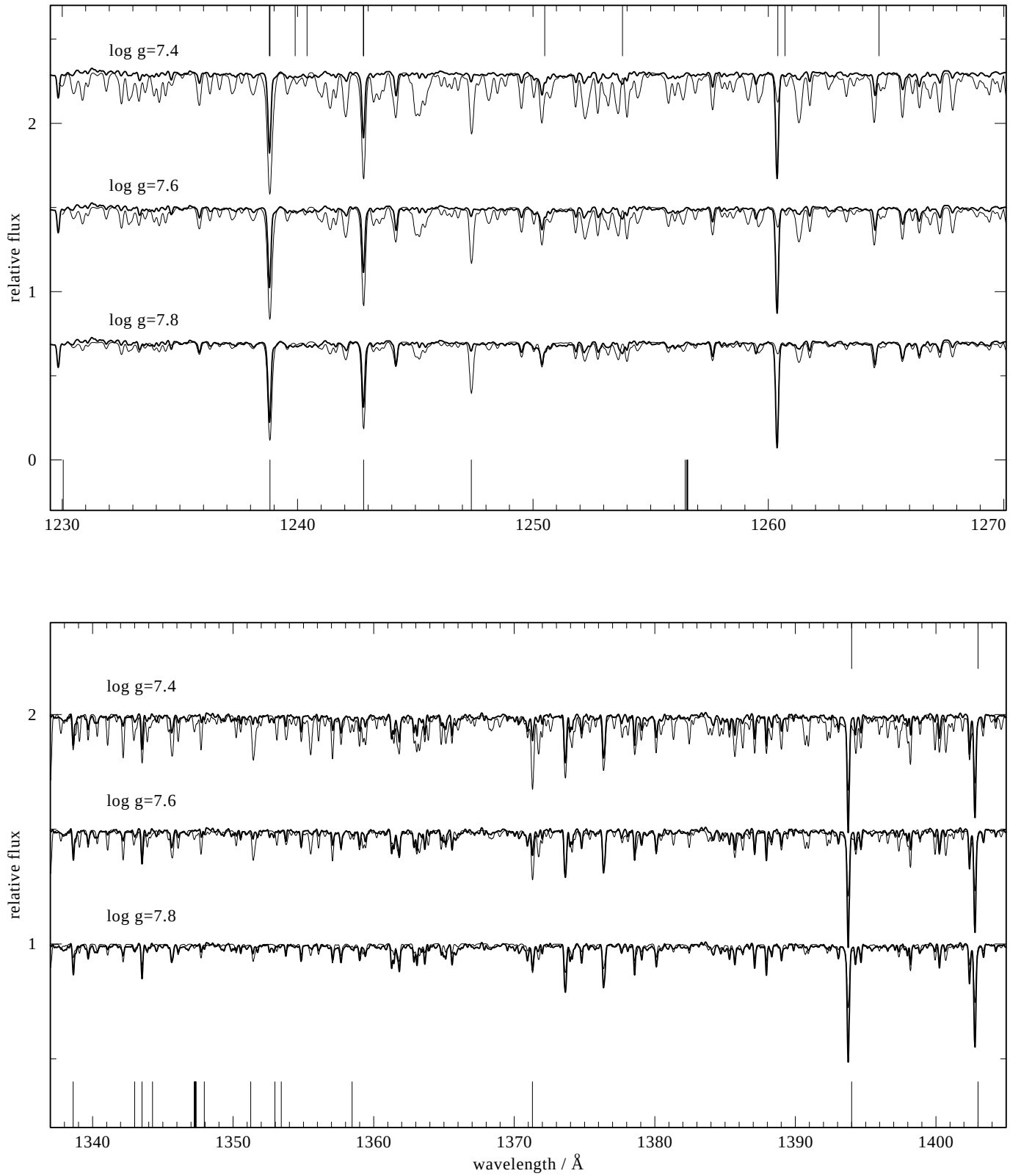

Fig. 4. Combined STIS spectrum of G 191-B2B (thick line) compared to our self-consistent NLTE model atmospheres ($\log g = 7.6$) with three effective temperatures (from *top* to *bottom* in each plot $T_{\rm eff}$=59 000, 56 000, 53 000 K): *Upper plot:* region dominated by Ni V lines; lower plot: region dominated by Fe V lines. Interstellar lines are indicated at the *top*, stellar C, N, O, and Si lines are indicated at the *bottom*

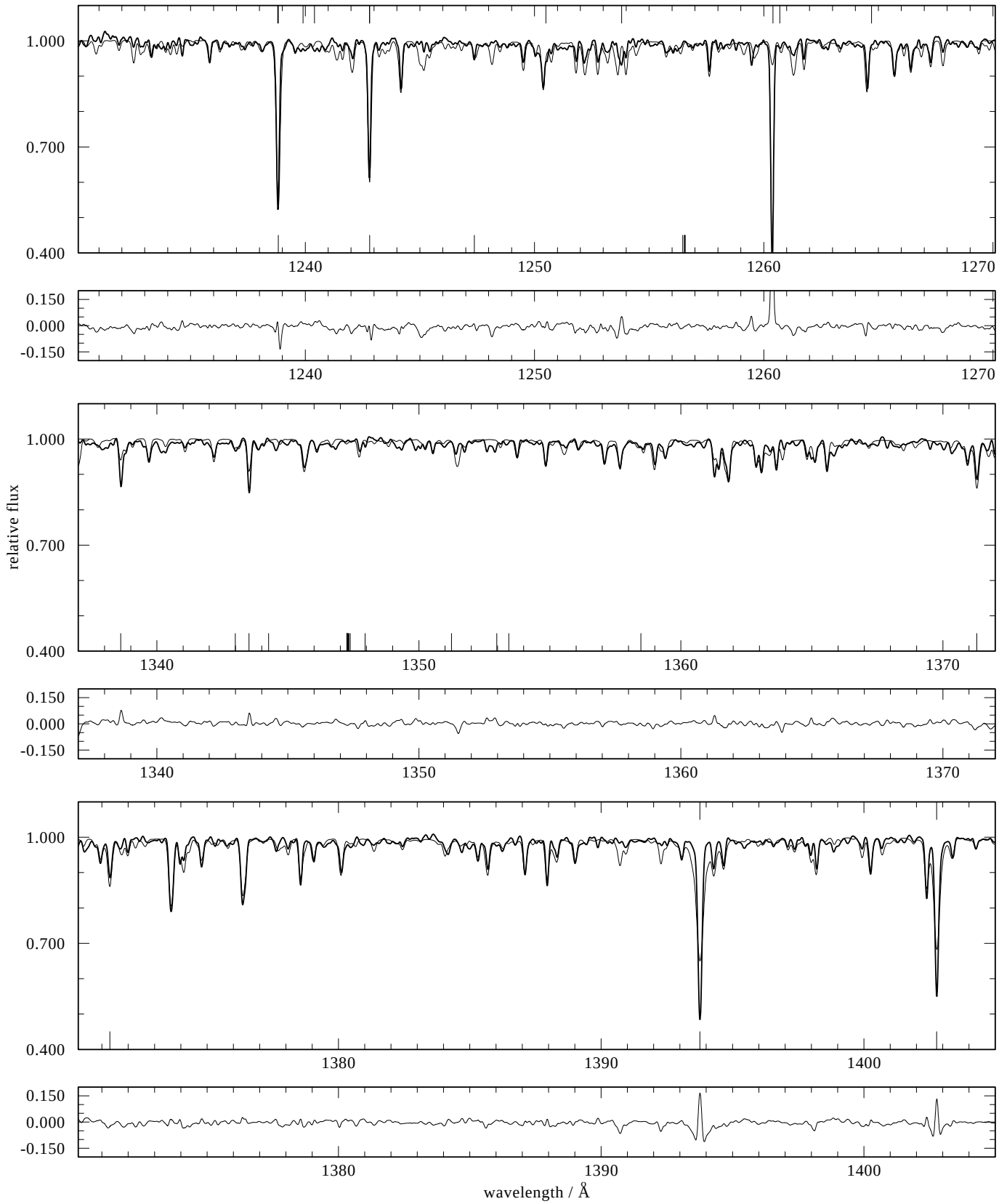

Fig. 5. Combined STIS spectrum of G 191-B2B (thick line) compared to our scaled NLTE model atmospheres ($T_{\rm eff}$=56 000 K, $\log g = 7.6$). *Upper plot:* region dominated by Ni V lines; *lower two plots*: regions dominated by Fe V lines. Interstellar lines are indicated at the *top*, stellar C, N, O, and Si lines are indicated at the *bottom*. The difference Theory-Observation is plotted in the *small panels*

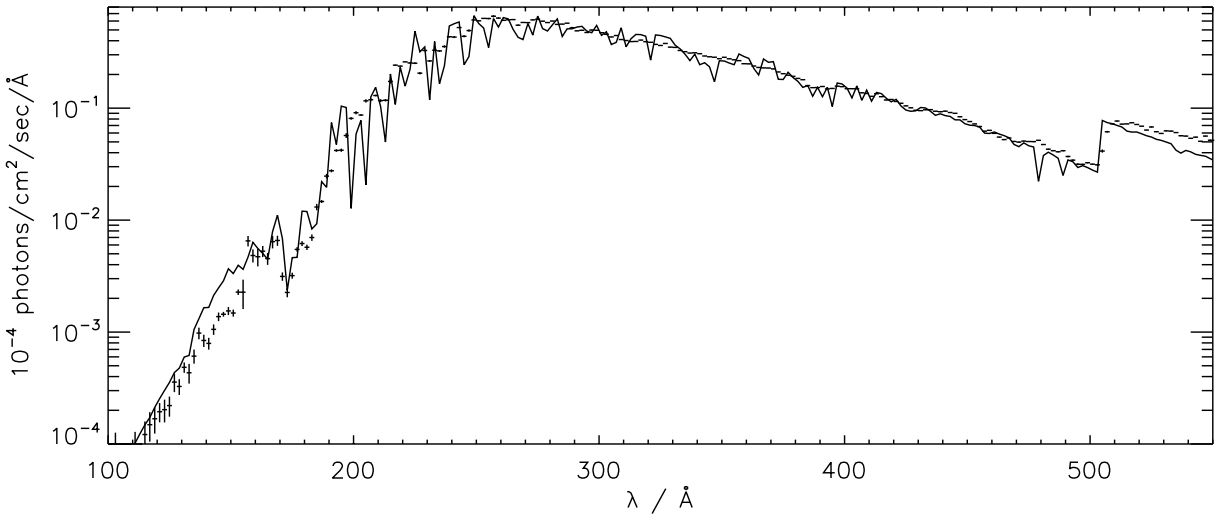

Fig. 6. EUVE spectrum of G 191-B2B (error bars) compared with a self-consistent diffusion model with $T_{\rm eff} = 56000\,{\rm K}$ and $\log g = 7.6$. The interstellar absorption is $N({\rm HI}) = 2.11 \cdot 10^{18}\,{\rm cm}^{-2}$, $\mathrm{He\,I/H\,I} = 0.067$, and $\mathrm{He\,II/H\,I} = 0.052$

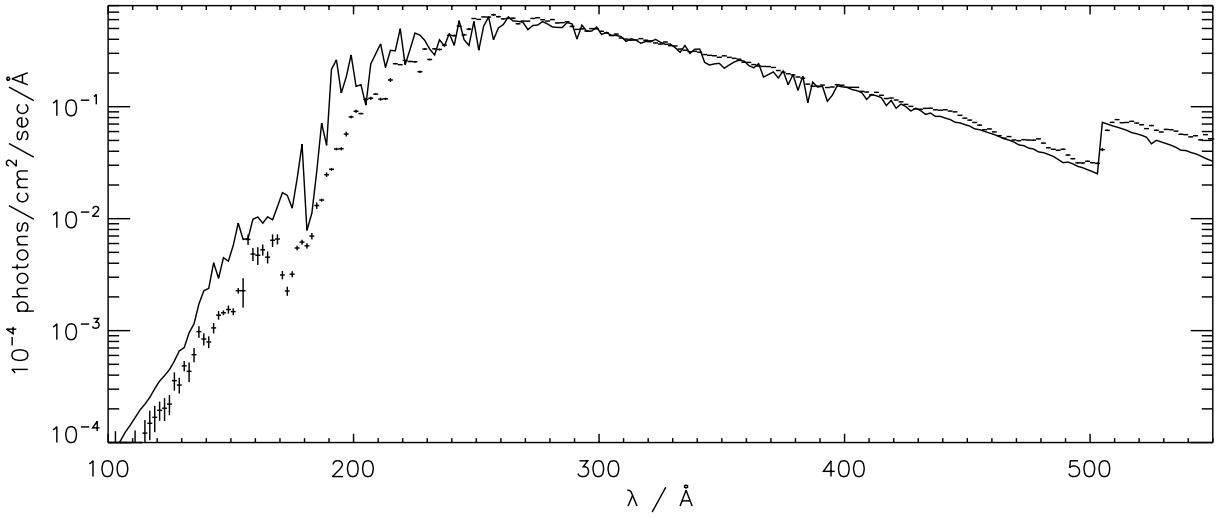

Fig. 7. EUVE spectrum of G 191-B2B compared with a model with homogeneous abundances (number fraction) of $\mathrm{C} = -5.7$, $\mathrm{N} = -5.4$, $\mathrm{O} = -6.0$, $\mathrm{Fe/H} = -5.0$, and $\mathrm{Ni} = -6.0$. $T_{\rm eff}$, $\log g$, and interstellar parameters are identical with Fig. 6

The homogeneous model can reproduce the EUVE spectrum at medium and long wavelengths. However, the synthetic flux is too high at all wavelengths shorter than $\approx$ 230 Å. The fit at $\approx$ 200–230 Å can be improved if an interstellar He II abundance of $\mathrm{He\,II/H\,I} \approx 0.2$ or an equivalent photospheric abundance is assumed (Lanz et al. 1996, Wolff et al. 1998) but this cannot remove the deviations at shorter wavelengths. As can be seen from Fig. 6, the diffusion model resolves this problem.

4. Discussion

The self-consistent calculation of atmospheric structure and element distribution results in a chemical stratification of the photosphere. This changes the shape of the EUV spectrum compared to homogeneous models so that the EUVE observations of G 191-B2B can now be reproduced without assuming any additional photospheric or interstellar absorbers. The required abundance profile is a straightforward product of the combined effects of diffusion and radiative levitation. It is not necessary to assume further mechanisms to account for the depletion of iron in the outer layers.

The self-consistent model can also reproduce the UV lines of iron and, with some restrictions, nickel which are the main sources of the EUV opacity. The agreement between the UV and EUV shows that these elements are indeed supported by radiative levitation and that this process is the dominant mechanism for providing photospheric traces of iron and nickel in G 191-B2B. This is a very important result since it has been assumed for several white dwarfs that mechanisms like mass-loss or accretion are necessary to account for the observed element abundances (e.g. Chayer et al. 1995a, Holberg et al. 1997, Barstow et al. 1999). Our analysis shows that, in the case of iron and nickel in G 191-B2B, other mechanisms are not necessary. This

result is in very good agreement with Unglaub & Bues (1998) who found that the absence of mass loss or a mass loss rate well below the critical value of $\dot{\mathrm{M}}= 10^{-14}\,\mathrm{M}_{\odot}$/yr is a prerequisite to observe stratified atmospheres. Mass loss rates above that critical limit, corresponding to T_{eff} above $\approx 65\,000$ K at a surface gravity of $\log g = 7.6$, produce a nearly homogeneous element composition. The effective temperature of G191-B2B is about 10 000 K below that value. The result is also in qualitative agreement with that of Chayer et al. 1997 who also found that a mass loss rate below $\dot{\mathrm{M}}= 10^{-16}\,\mathrm{M}_{\odot}$/yr results in an abundance stratification, in this case of Si, that is essentially given by the equilibrium radiative levitation theory. The increasing effect of mass loss on the chemical composition should become visible in the slightly hotter counterparts of G 191-B2B.

Acknowledgements. The authors would like to thank D. Koester (Kiel) and K. Werner (Tübingen) for useful discussions and comments. This work has been supported by the Deutsches Zentrum für Luft- und Raumfahrt (DLR) under grant 50 OR 96173. We have made use of the Simbad data base, operated at CDS, Strasbourg, France. Model atmospheres have been calculated on CRAY machines of the Rechenzentrum Kiel.

References

Barstow M.A., Hubeny I., 1998, MNRAS 299, 379
Barstow M.A., Fleming T.A., Diamond C.J., et al., 1993, MNRAS 264, 16
Barstow M.A., Hubeny I., Lanz T., Holberg J.B., Sion E.M., 1996a, In: Bowyer S., Malina R.F. (eds.) Astrophysics in the Extreme Ultraviolet. Kluwer, Dordrecht, p. 185
Barstow M.A., Holberg J.B., Hubeny I., et al., 1996b, MNRAS 279, 1120
Barstow M.A., Dobbie P.D., Holberg J.B., Hubeny I., Lanz T., 1997, MNRAS 286, 58
Barstow M.A., Hubeny I., Holberg J.B., 1999, In: Solheim J.E. (ed.), Proceedings of the 11^{th} European Workshop on White Dwarfs, in press
Bruhweiler F., Kondo Y., 1981, ApJ 248, L123
Chayer P., Fontaine G., Wesemael F., 1989, In: Wegner G. (ed.) White Dwarfs. Springer, Berlin, p. 253
Chayer P., Fontaine G., Wesemael F., 1991, In: Vauclair G., Sion E. (eds.) White Dwarfs. Kluwer, Dordrecht, p. 249
Chayer P., LeBlanc F., Fontaine G., et al., 1994, ApJ 436, L161
Chayer P., Fontaine G., Wesemael F., 1995a, ApJS 99, 189
Chayer P., Vennes S., Pradhan A.K., et al., 1995b, ApJ 454, 429
Chayer P., Fontaine G., Pelletier C., 1997, In: Isern J., Hernanz M., Garcia-Berro E. (eds.) White Dwarfs. Kluwer, Dordrecht, p. 253
Dreizler S., 1999, In: Schielicke R.E. (ed.) Reviews in Modern Astronomy 12, in press
Dupuis J., Vennes S., Bowyer S., Pradhan A.K., Thejll P., 1995, ApJ 455, 574
Holberg J.B., Hubeny I., Barstow M.A., et al., 1994, ApJ 425, L105
Holberg J.B., Barstow M.A., Lanz T., Hubeny I., 1997, ApJ 484, 871
Jordan S., Wolff B., Koester D., Napiwotzki R., 1994, A&A 290, 834
Koester D., 1989, In: Wegner G. (ed.) White Dwarfs. Springer, Berlin, p. 206
Koester D., 1996, In: Bowyer S., Malina R.F. (eds.) Astrophysics in the Extreme Ultraviolet. Kluwer, Dordrecht, p. 185
Lanz T., Barstow M.A., Hubeny I., Holberg J.B., 1996, ApJ 473, 1089
Marsh M.C., Barstow M.A., Buckley D.A., et al., 1997, MNRAS 287, 705
Morvan E., Vauclair G., Vauclair S., 1986, A&A 163, 145
Rumph T., Bowyer S., Vennes S., 1994, AJ 107, 2108
Sion E.M., Bohlin R.C., Tweedy R.W., Vauclair G.P., 1992, ApJ 391, L29
Unglaub K., Bues I., 1998, A&A 338, 75
Vauclair G., 1987, In: Philip A.G.D., Hayes D.S., Liebert J.W. (eds.) IAU Colloquium No. 95, The Second Conference on Faint Blue Stars. L. Davis Press, Schenectady, p. 341
Vauclair G., 1989, In: Wegner G. (ed.) White Dwarfs. Springer, Berlin, p. 176
Vauclair G., Vauclair S., Greenstein J.L., 1979, A&A 80, 79
Vennes S., Chayer P., Thorstensen J.R., Bowyer S., Shipman H.L., 1992, ApJ 392, L27
Vennes S., Chayer P., Hurwitz M., Bowyer S., 1996, ApJ 468, 898
Vidal-Madjar A., Allard N.F., Koester D., et al., 1994, A&A 287, 175
Werner K., Dreizler S., 1994, A&A 286, L31
Wolff B., Jordan S., Koester D., 1996, A&A 307, 149
Wolff B., Koester D., Vidal-Madjar A., 1997, In: Isern J., Hernanz M., Garcia-Berro E. (eds.) White Dwarfs. Kluwer, Dordrecht, p. 199
Wolff B., Koester D., Dreizler S., Haas S., 1998, A&A 329, 1045
Wolff B., Koester D., Dreizler S., 1999a, In: Solheim J.E. (ed.) Proceedings of the 11^{th} European Workshop on White Dwarfs. in press
Wolff B., Koester D., Lallement R., 1999b, A&A, in press